Amorphization and energy maps of mechanically alloyed FeSiB-based alloys

(article starts on next page)

Amorphization and energy maps of mechanically alloyed FeSiB-based alloys

T. Larimian [a], V. Chaudhary [b,c], R.K. Gupta [d], R.V. Ramanujan [b], T. Borkar [a,*]

[a] *Mechanical Engineering Department, Cleveland State University, Cleveland, OH, 44115, USA*
[b] *School of Materials Science and Engineering, Nanyang Technological University, 639798, Singapore*
[c] *Industrial and Materials Science, Chalmers University of Technology, SE-41296, Gothenburg, Sweden*
[d] *Department of Materials Science and Engineering, North Carolina State University, Raleigh, NC-27606, USA*

ABSTRACT

In this research work, the effect of different mechanical alloying processing parameters such as ball-to-powder weight ratio (BPR), size of the milling balls, rotation speed, and milling duration on the amorphization of an elemental blend of iron (Fe), silicon (Si), and boron (B) have been studied. FeSiB powder alloys were obtained by mechanically alloying of elemental powders for 10, 20, and 30 h with a rotation speed of 700 rpm, stearic acid as process control agent (PCA), and the ball-to-powder ratio of 5:1, 10:1, and 15:1. The resultant powders were then consolidated using the spark plasma sintering (SPS) technique. The effect of SPS processing parameters on mechanical and magnetic properties was studied. For samples milled under the same conditions, the saturation magnetization of the samples sintered at higher temperatures was proven to be higher. Moreover, the effect of heat treating the amorphous powder alloy before SPS processing was studied. The results showed an increase in the saturation magnetization of the heat-treated samples but also an increase in coercivity. Finally, the energy maps were drawn for mechanically alloyed FeSiB-based samples milled under different conditions to find the window for the total energy and minimum energy of a single ball that would give us an amorphous structure useful for magnetic properties.

1. Introduction

Iron-based magnetic materials are the subject of many scientific studies due to their broad application in sensing devices, power electronics, energy-efficient transformers, and even in everyday devices such as mobile phones, smart watches, computer hard disks, etc. [1–3]. These alloys have excellent magnetic properties, such as low magnetic loss, coercivity and fast flux reversal, and high permeability and saturation magnetization [4,5]. The demand for developing soft magnetic alloys with improved performance has increased recently due to the high need for energy-saving devices and the electrification of transport systems.

Magnetic alloys made of the 3 main elements of iron (Fe), silicon (Si), and boron (B) possess excellent soft magnetic properties (e.g., high permeability and saturation magnetization along with low coercivity), which is the primary reason for selecting these alloys for further investigations [5]. In most cases, the magnetic properties, such as permeability and saturation flux of the FeSiB-based alloys, are better than those of other magnetic alloys, such as amorphous cobalt-based alloys or Si-Steel [6]. Researchers have studied the reason for the good magnetic properties of these alloys and concluded that the presence of α-Fe(Si) grains dispersed in an amorphous iron matrix is mainly

responsible for their excellent magnetic properties [7]. The addition of elements such as niobium and copper significantly affects the appearance of the α-Fe(Si) grain and the overall improvement of magnetic and mechanical properties of the FeSiB-based alloys [8,9]. Amorphous metallic alloys have been the subject of many studies due to their excellent corrosion and wear resistance and outstanding mechanical properties, such as high yield strength and low elastic modulus compared to crystalline metallic alloys [7,10–13].

Until recently, the primary way of fabricating amorphous metallic alloys was rapid cooling/quenching. In this way, the metal was either cooled to a temperature below its crystallization temperature with a very high cooling rate of 10^6 to 10^{10} k/s or prepared by condensing the vapor into a cold substrate [14,15]. However, these processes need help producing bulk materials, and materials can only be fabricated in thin ribbons or wires. The thickness of such ribbons is typically ~50 μm [13], and therefore, they need to be stacked on top of each other to make magnetic components for real applications. The shapes of the magnetic parts produced with this technique are limited to the shapes and sizes that can be machined from the stack of ribbons. Moreover, these ribbons are pretty brittle, complicating the fabrication of magnetic components with complex shapes [16]. Therefore, there is a critical need to investigate the processing routes to not only increase the efficiency of the

---

produced magnetic alloys but also miniaturize them for applications in electric and electronic equipment, especially for next-generation environmentally friendly electric and hybrid cars.

Mechanical alloying (MA) is a powerful alternative for the fabrication of amorphous magnetic alloys [17]. Such powder alloys can be consolidated into bulk magnetic parts via spark plasma sintering (SPS). SPS processing parameters can affect the magnetic and mechanical properties of the resultant parts. In general, SPS-fabricated parts have uniform grain structures and are high-density, affecting the permeability and saturation magnetization of the processed parts [18,19]. However, only a few researchers have investigated the sintering of soft magnetic alloys, and therefore, the effect of the processing parameters on the microstructure, mechanical, and magnetic properties of the sintered alloys still needs to be fully understood and investigated.

There are only a few research done on sintering soft magnetic alloys; therefore, the effect of the processing parameters on the sintered alloys is not yet fully understood. A few researchers have studied the effect of temperature and holding time on similar compositions. Xio et al. [20] have worked on FeSiCuNb composition and proven that the sintering temperature influences both saturation magnetization (M_s) as well as coercivity (H_c). They found that increasing the sintering temperature increases the saturation magnetization while the coercivity decreases with higher temperatures. Due to the presence of boron and the possibility of the formation of boron phases in our samples and the fact that boron phases such as Fe_2B, Fe_3B, or $Fe_{23}B_6$ can negatively affect the Ms and increase the Hc values and overall deteriorate the magnetic properties, interpreting the results from our research work can be more challenging. Moreover, Neamtu et al. [21] studied the role of holding time on SPS-processed FeSiB alloys at low pressures. In order to achieve full densification at a low pressure, they increased the sintering temperature up to 800 °C, and they realized that as a result of better densification at higher temperatures, the magnetic properties of the alloy improved. Another factor that can affect the SPS-fabricated parts is the pressure. Gheiratmand et al. [19] worked on the sintering of Finemet at low pressures and high holding times. They realized that the density of the fabricated part depends on whether the initial powder was amorphous or partially crystallite (Higher density in case of amorphous powder). However, choosing higher holding times will increase the chance of crystallization. Xio et al. [20] found that if the loading pressure is less than 500 MPa the powders would not be consolidated or may require longer holding times to achieve full densification. Neamtu et al. [21] did SPS on FeSiB composition with a holding time of 1–15 min with varying temperatures with pressure of 30 MPa. They did their sintering experiment at temperatures from 450 to 900 °C as their pressure was too low; they only achieved full compactions at temperatures over 800 °C. Therefore, in this research work, we have used the high compaction pressure of 600 MPa to decrease the holding time or sintering temperature to achieve full densification.

During the mechanical alloying process, several different processing parameters can affect the amorphization process, as well as the total energy involved in the process and the energy associated with milling balls. The milling processing parameters, such as the size of the balls, the ball-to-powder weight ratio, the rotation speed, the milling duration, and even the process control agent, can affect the amorphization. Therefore, we have attempted to investigate the effect of these processing parameters on the amorphization of FeSiB powder alloy. We investigated the effect of mechanical alloying on amorphization, microstructure, phase transformation, and mechanical and magnetic behavior of Fe-Si-B-based alloys processed via the SPS process. This study will open new avenues for the processing and developing bulk amorphous and nanocrystalline magnetic alloys.

2. Experimental details

$Fe_{77.5}Si_{13.5}B_9$ alloy was prepared by Fritsch Pulverisette 7 high energy planetary ball milling using elemental powders where both milling balls and bowls were made of tungsten carbide. The powders used in these experiments were iron powder with a purity of 99.9 % and size of 1–9 μm, silicon with a purity of 99.99 % and mesh size of −325, and amorphous boron with a purity of 97 %. $Fe_{77.5}Si_{13.5}B_9$ was milled for 10, 20, and 30 h with the ball-to-powder ratios of 5:1, 10:1, 15:1, and 700 rpm as the rotation speed. To prevent oxidation during milling, the elemental powders were loaded and sealed in milling bowls in a glove box filled with argon gas. To avoid cold welding during milling, 2 wt% of stearic acid was added to the process control agent (PCA). To prevent the powder from overheating during the mechanical alloying process, we put 10 min pauses in between each of the 10 min milling durations.

The Spark Plasma Sintering process was performed under an argon atmosphere, and powder was pre-compacted using tungsten carbide dies and punches at a pressure of 20 MPa. The maximum pressure in the process was 600 MPa, the holding time was 5 min, and the temperatures used were 470 °C and 510 °C at the constant heating rate of 30 °C/min. Differential scanning calorimetry (DSC) was performed to find the crystallization temperatures of different phases in the alloy powder. SPS-processed bulk samples were mounted and polished using different-grade polishing papers and then imaged using an FEI-Quanta Nova-SEM. The Microhardness of the samples was measured using Vickers standard under load of 5N and dwell time of 10s. 10 measurements from 10 different spots were taken for each sample, and the average values were reported. The annealing process was performed at a temperature of 200 °C for 2 h.

The magnetic properties were measured using a magnetometer (VSM-Lakeshore 7404) with a maximum magnetic field of 1 T. X-ray diffraction (XRD) using a Rigaku Ultima III X-Ray diffractometer (Cu Kα radiation, 1.54 Å) was done to determine the phase(s) of the samples. The crystallite sizes of the samples were measured using the linear Williamson-Hall method and based on the XRD data acquired from each sample.

3. Results and discussion

3.1. Mechanical alloying parameters and their effect on amorphization of FeSiB

The mechanical alloying process has gained significant attention due to its simplicity and ability to produce amorphous alloys through solid-state amorphization instead of conventional rapid solidification [22]. Other researchers have achieved the amorphization of alloys with different compositions [23–26], but this research aims to study the amorphization of FeSiB-based alloys via the mechanical alloying process. The reason for choosing the mechanical alloying process for achieving amorphization for our FeSiB-based alloys is due to its wider glass forming range as compared to conventional methods such as liquid metallurgy [27]. The amorphization process via mechanical alloying is affected by multiple different processing parameters. These parameters include the duration of milling, the ball-to-powder weight ratio, rotation speed, the size of the milling balls, and even the PCA that is used during the process. We studied each of the mentioned parameters by designing experiments where the processing parameters were changed one at a time while the rest of the parameters were kept the same to investigate the role of each parameter on the amorphization of the alloyed powder. Our previous research on FeSiB-based alloys milled with rotation speeds of 350 and 500 rpm and longer milling durations of up to 120 h revealed that full amorphization only occurred in one sample (FINEMET milled with rotation speed of 350 rpm, BPR 10:1 and ball size 3 mm) which is why we chose to change the mechanical alloying processing parameters to achieve amorphization at lower milling duration. Therefore, we studied the amorphization process under a much higher rotation speed for the next step of our research work. For this reason, the higher rotation speed of 700 rpm and milling durations of 10–30 h were chosen for the new set of experiments. Additionally, to understand the effect of ball size on the amorphization process, two different sizes of milling

balls (3 and 6 mm) were used.

The XRD patterns of 10 different FeSiB samples that were milled with the rotation speed of 700 rpm, milling durations of 10–30 h, ball sizes of 3 and 5 mm, and ball-to-powder ratios of 5:1, 10:1, and 15:1 are depicted in Fig. 1. From these XRD patterns, the highest level of amorphization is observed in a sample milled for 30h, with a BPR of 10:1 and a ball size of 3 mm. The XRD patterns of the rest of the samples showed the highest level of amorphization and lowest crystallite sizes for the following samples: BPR 10:1, milling duration 20h with 3 mm balls, BPR 10:1 milling duration 10h with 5 mm balls, BPR 15:1 milling duration 10h with 3 mm, BPR 15:1 milling duration 10 with 5 mm balls and BPR 5:1, milling duration 20h with 5 mm balls in sequence. From Fig. 1, it can be observed that choosing a low BPR of 5:1 does not result in a fully amorphous powder; however, in some cases, a certain level of broadening is observed in powders milled with BPR 5:1. It can also be concluded that in comparison between powders processed with the same milling duration and ball size, powders that were milled with BPR 10:1 showed the most promising results.

Fig. 2 shows the XRD patterns of mechanically alloyed FeSiB powders using the same rotation speed and ball size but with different ball-to-powder ratios and milling durations. When comparing samples that were milled with the same milling duration of 10 h, it can be observed that even though both samples show a certain level of amorphization, the sample milled with medium BPR 10:1 depicts broader diffraction peaks and smaller crystallite sizes. It suggests that the amorphization process is negatively affected when BPR is high (15:1) or low (5:1). In case of high BPR, the higher number of balls can increase the number of collisions during the milling process, which can consequently increase the amount of excess heat that is generated during the alloying process. This excess heat can negatively affect the amorphization process and result in more crystallization [23]. On the other hand, for low BPR, enough kinetic energy is not transferred to the powder during the mechanical alloying, hindering the amorphization process.

3.2. The effect of ball size on the amorphization of FeSiB alloys

In order to study the ball size effect on amorphization, FeSiB alloy powders were milled with the same rotation speed (700 rpm) but 3 different BPRs, 3 different milling durations, and 2 different sizes of milling balls. We have observed from these 4 different experiments that
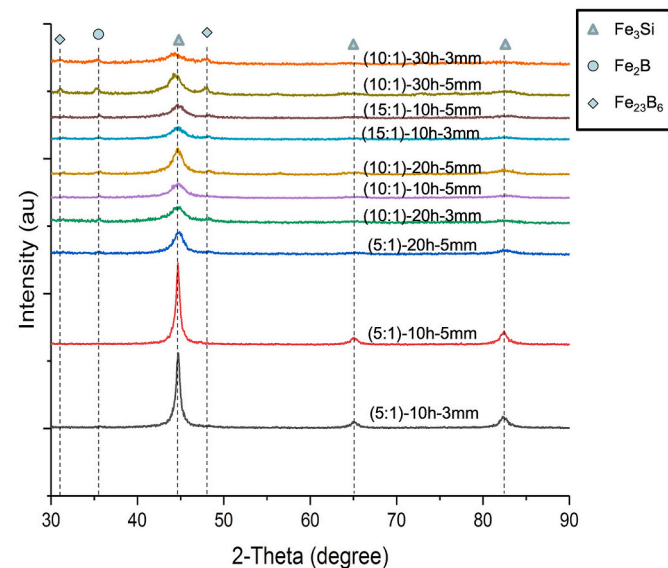
Fig. 2. XRD patterns of FeSiB powder mechanically alloyed with a Rotation Speed of 700 rpm and ball size of 5 mm but different milling durations and ball-to-powder ratios.

powders milled using 3 mm balls showed higher levels of amorphization than powders milled with 5 mm balls. This comparison can be observed from the XRD patterns of samples depicted in Figs. 2 and 3. Both show XRD patterns of samples that were milled with the BPR 10:1 and 30 h milling time, samples with BPR 15:1 and 10h milling time, and samples with BPR 10:1 and milling time 20 h, but samples depicted in Fig. 2 were milled with 5 mm balls whereas samples depicted in Fig. 3 were milled with 3 mm balls. It can be observed that samples that were milled using the 3 mm milling balls show broader diffraction peaks and higher levels of amorphization. This is due to the intense friction when smaller balls are used [28]. Also, a higher milling duration results in a higher level of amorphization. This can be observed by comparing samples that were milled with BPR 10:1 and 30 or 20 h milling duration as well as samples

Fig. 1. XRD patterns of FeSiB powder mechanically alloyed with a Rotation Speed of 700 rpm and different milling duration, ball-to-powder ratio, and ball size.
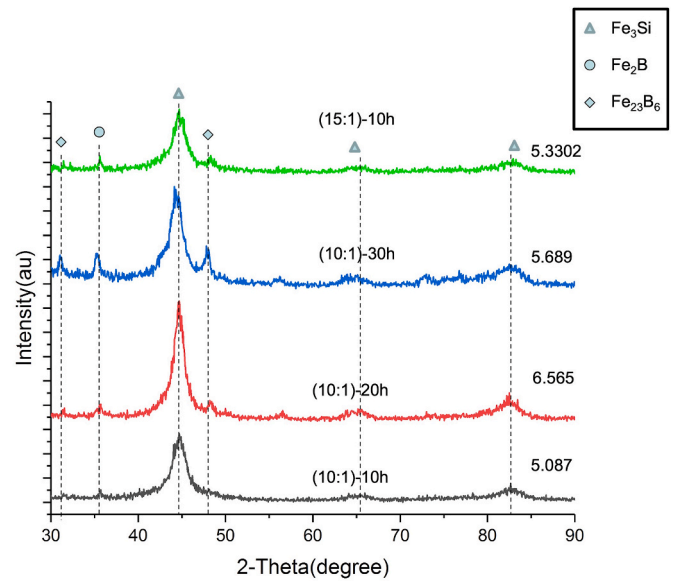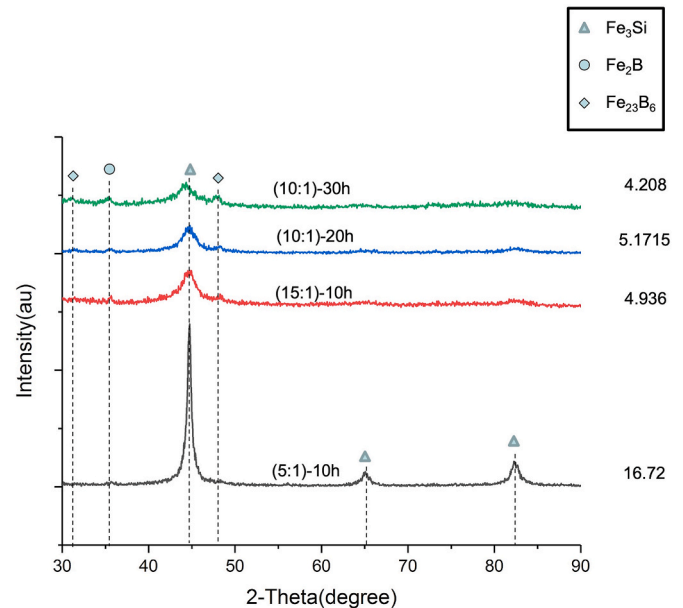
Fig. 3. XRD patterns of FeSiB powder mechanically alloyed with a Rotation Speed of 700 rpm and ball size of 3 mm but different milling durations and ball-to-powder ratios.

milled with 5 mm ball size with BPR 5:1 and 10 or 20 h where in all cases, higher milling duration results in higher amorphization levels. From the XRD patterns depicted in Fig. 3, it can be observed that for the powder milled with 700 rpm and BPR 10:1, the broadening of the peaks has already started at 20 h of milling, but full amorphization does not occur until 30 h of milling. From the XRD patterns depicted in Fig. 1, it can be observed that full amorphization was achieved after 30 h of milling. However, it is worth mentioning that if the milling duration is too long, powders' amorphous structure can return to a crystalline state. This phenomenon was observed in our previous research work on FeSiB samples that were milled with a powder ratio of 10:1, with a ball size of 3 mm, rotation speed of 350 rpm, and milling durations of 30, 60, and 90 h [9]. While the sample milled for 30 h did not show signs of amorphization, the 60 h and 90 h milled samples showed some levels of amorphization. However, based on the XRD pattern depicted in Fig. 4, the 60h sample shows the most amorphous microstructure, while the sample that was milled for 90 h is almost back to its crystalline structure.

3.3. Process control agent optimization

Process control agent (PCA) is another factor that can affect the amorphization during the mechanical alloying process. For this study, two different PCAs (stearic acid and benzene) were used to investigate their effect on the amorphization process. Iron, silicon, and boron powders with the same composition were placed inside identical milling bowls using identical ball sizes (3 mm), milled with the same rotation speed, the ball-to-powder ratio and milling duration with one bowl using stearic acid as PCA, and the other using benzene. The XRD patterns obtained from both proved that stearic acid is the superior choice for our mechanical alloyed FeSiB samples in terms of level of amorphization as well as carbon contamination traced in the samples (Fig. 5). Therefore, we have selected stearic acid as PCA for further investigation on FeSiB samples milled with the rotation speed of 700 rpm. A comprehensive study on mechanical alloying of iron-based amorphous alloys done by Neamtu et al. [1], using Fe, Si, and B as their elemental powders, showed the importance of the PCA agent in the amorphization process. According to their study, amorphization of iron-based soft magnetic alloys can only be done when a process control agent (PCA) is used. They have also argued that the carbon atoms provided by the decomposition of the PCA agent help with the amorphization process. Nouri et al. [2] proposed that the PCA agent changes the composition of the milled material due to severe thermodynamic conditions during the mechanical alloying process. Neamtu et al. [29] correlated the success of the wet mechanical
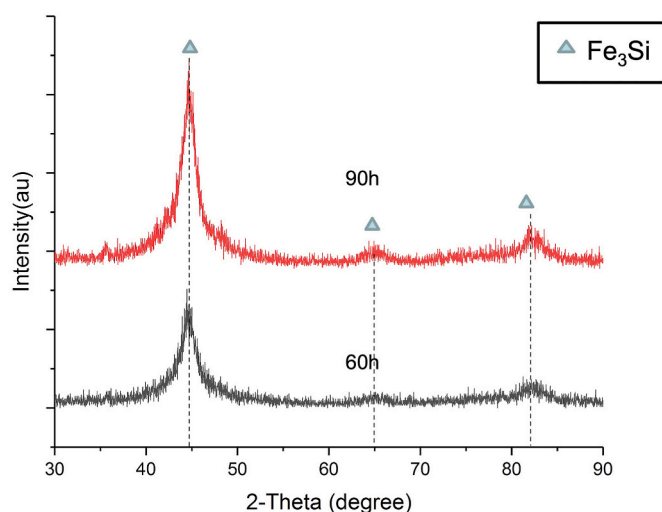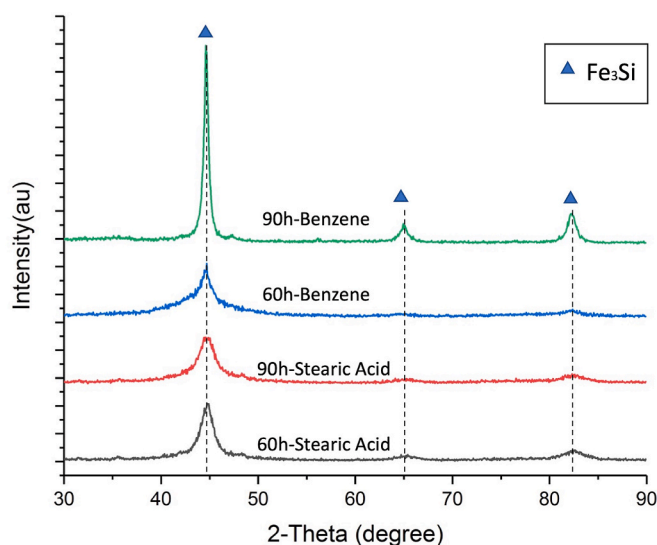

Fig. 5. XRD patterns of mechanically alloyed FeSiB powder using Benze and stearic acid as process control agents.

alloying (with the use of the PCA agent) to the carbon contamination that occurs during the process due to the results they observed from the x-ray diffraction patterns of the ribbons they wet milled for 20 h. Neamtu et al. [29] stated that since carbon atoms are metalloid atoms, their existence aids the amorphization process. According to studies by Nouri et al. [30], oxygen and carbon are the most common atomic species that have contaminated the milled powders. Even though oxygen contamination can lower the crystallization temperature, according to Koch et al. [23], the overall effect of PCA agents is positive on the amorphization process. Suryanarayana [17] explained that this phenomenon occurs due to small carbon atoms penetrating the interstitial sites and consequently destroying the order of the lattice and destabilizing the crystal phase [17].

3.4. Energy maps (effect of ball milling energy on amorphization)

The amorphization process during the mechanical alloying process and the glass-forming ability of the blend of elemental powder composition are affected by the amount of energy introduced to the powder during milling. Mechanical alloying processing parameters such as milling duration, ball-to-powder ratio, ball size, and rotation speed are among the factors that directly influence the amount of energy induced into the powder during milling. To understand the effect of these processing parameters on the milled powder, these factors were converted into two parameters measuring the energy of a single milling ball and the total energy introduced to the powder during the milling process [31]. We have designed energy maps for FeSiB-based alloys based on these two parameters. *We experimented on FeSiB-based powder alloys under various mechanical alloying conditions, calculated the impact energy of a single ball as well as the total energy that is introduced to the powder during the process, and studied the correlation between these two energy parameters with whether a powder alloy has amorphous structure. This study aims to determine the potential window of total energy in which the milled powder would have an amorphous structure. Additionally, we have discovered a minimum value for the impact energy of a single ball below which amorphization does not take place even if the total energy introduced to the powder during the milling process is in the amorphization window.*

The formula for kinetic energy is $K = 0.5mv^2$. The kinetic energy of a single ball can be calculated as [32]:

$$E_b = 0.5m_b v_b^2 \qquad \text{(Equation 1)}$$

Fig. 4. XRD patterns of FeSiB powder mechanically alloyed with a Rotation Speed of 350 rpm, the ball-to-powder ratio of 10:1, a ball size of 3 mm with milling durations of 60 and 90 h.

Where, E_b is the energy of a single ball, m_b is the mass of a ball, and v_b is the absolute velocity of the ball. As mentioned before, when there are multiple balls present during the mechanical alloying process, the energy of each ball is a factor of the energy of the ball as if it is alone in the bowl. The energy of a single ball when there are multiple balls in the bowl can be written as [31]

$$E_b{'} = \phi_b E_b \qquad \text{(Equation 2)}$$

where:

$$\phi_b = 1 - n_v{}^\epsilon \qquad \text{(Equation 3)}$$

The ϵ factor equals 1.193 for 3 mm balls and 1.462 for 5 mm balls (calculated based on formula A21 from Ref. [33]). The variable ϕ_b is dependent upon the packing fraction (n_v), which depends on the ratio of the number of balls used during the specific mechanical alloying process and the total number of milling balls that can fit inside the milling bowl. Therefore, if the number of balls used in an experiment is given by n_b and the total number of balls that can fit inside a milling bowl is presented by $n_{b.v}$ the packing fraction (n_v) can be written as

$$n_v = \frac{n_b}{n_{b.v}} \qquad \text{(Equation 4)}$$

According to Burgio et al. [34], the total number of balls that can be fitted inside the milling bowl in a simple cubic arrangement can be written as:

$$n_{b.v} = \frac{\pi D^2 H}{4d^3} \qquad \text{(Equation 5)}$$

where D and H are the diameter and height of the milling bowl, and d is the diameter of each ball. For the next step, we calculated the total energy transferred to the powder unit mass during the mechanical alloying process. The total energy per unit mass depends on the frequency (f) of collision between the balls, the energy of a single milling ball ($E_b{'}$), the total number of balls in the milling process (n_b), and the milling duration (t) [31]. The formula for calculating the total energy of the process can be written as:

$$E_t = \frac{f t n_b E b{'}}{m_p} \qquad \text{(Equation 6)}$$

In this equation m_p is the mass of powder being milled. The frequency of impact for a single ball has been calculated by Iasonna and Magini [33]:

$$F = K(\Omega - \omega) \qquad \text{(Equation 7)}$$

In this equation Ω is the rotation speed of the disk, ω is the rotation speed of the milling bowl and K is equal to 1.5. The milling machine used for all our experiments was Fritsch Pulverisette 7, for which the ratio of the disk's rotation speed to the vial's rotation speed is $\frac{\Omega}{\omega} = 2$.

In this study, the energy of a single ball and the total energy per unit mass are calculated for 19 different FeSiB-based alloys that were mechanically alloyed under different processing conditions. The processing parameters (ball size, milling duration, BPR, and rotation speed) are listed in Table 2. The XRD patterns of the first four powder samples, which showed amorphous structure, are depicted in Fig. 2. For all these samples with amorphous structures, higher rotation speeds and shorter milling durations of up to 30 h were used. However, the best result in terms of amorphization was observed after 30 h of milling. From XRD patterns, samples milled with the following milling parameters showed amorphous structure: BPR 10:1–30h milled-3mm balls, BPR 10:1–20h milled-3mm balls, BPR 10:1–10h milled-5mm balls, BPR 15:1–10h milled-3mm balls, BPR 15:1–10h milled-5mm balls, BPR 10:1–30h milled-5mm balls, BPR 10:1–20h milled-5mm balls and BPR 5:1–20h milled-5mm balls as well as one of our samples from our previous study on mechanical alloying of Finemet [8] with BPR 10:1, 120h milled, 3 mm balls.

The energy of a single ball, as well as the total energy introduced to the powder during the milling process for all 19 conditions, is depicted in Fig. 6. From Fig. 6, we located the spots representing the powder alloys that showed amorphous structure (based on XRD results) and discovered that all the FeSiB-based samples that show amorphous structure after mechanical alloying fall within the total energy window of 2462.13 Jh/g and 7386.3 Jh/g. From Fig. 6, it can also be observed that some samples that fall within the amorphization window (2462.13 Jh/g and 7386.3 Jh/g) do not show amorphous structure. These samples include powders that were milled with a rotation speed of 500 rpm with a BPR of 10:1 and a ball size of 3 mm with a milling duration of 60 and 90 h, as well as samples milled with a rotation speed of 350 rpm with a BPR of 15:1 and a ball size of 3 mm with 90- and 120-h milling duration. From this observation, we concluded that in order to reach the amorphous state, there is a minimum energy required for a single ball, and the powders in the amorphization window that did not have an amorphous structure all had the energy of a single ball below the required energy. From the energy map depicted in Fig. 6, all the samples that exhibited amorphous structure are above the line of 0.0029 J for the impact energy of a single ball. By using these energy maps, we can predict whether a FeSiB-based powder that is mechanically alloyed with any processing parameter will have an amorphous structure or not by taking into account the minimum requirement for E_b and the window of total energy in which the powder alloy shows an amorphous structure.

The powder alloys that have gone through the milling process are prone to residual stress introduced by the mechanical alloying process [35]. In this research work, we studied the effect of residual stress on the magnetic properties of alloys processed by mechanical alloying by experimenting on heat-treated (to reduce the residual stress) and non-heat-treated samples that were mechanically alloyed under the same condition. Neamtu et al. [29], who studied the mechanical alloying process, found that the saturation magnetization of milled magnetic alloys increased from ~131 to ~141 emu/g when the annealing heat treatment was done. Sinha et al. [36], who studied the role of annealing on magnetic properties of finemet alloys, observed similar results. Therefore, we performed the annealing of mechanically alloyed FeSiB samples and its effect on the magnetic properties. For these experiments, we chose an amorphous powder that was milled for 30 h using 700 rpm, 10:1 ball-to-powder ratio, and 3 mm balls. This powder was then divided into two similar amounts; one was heat treated at a temperature of 200 °C for 2 h, and the other was not heat treated. Fig. 9 shows the saturation magnetization and coercivity values for the two 30h-milled amorphous powders: one heat-treated and one not heat-treated. The coercivity value of the heat-treated sample is lower than the sample that
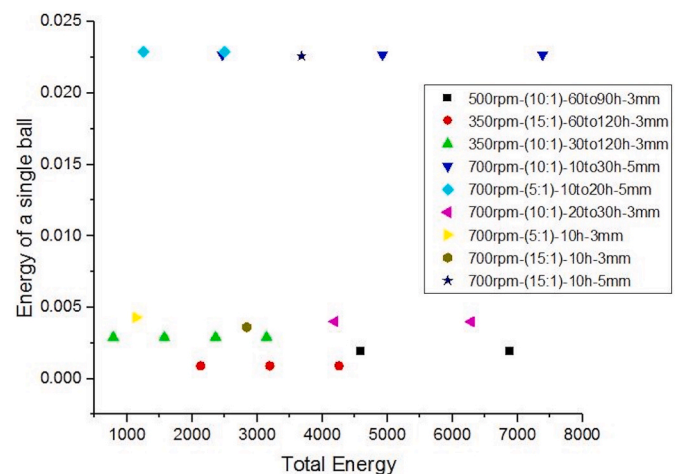

Fig. 6. Graph of Total energy (Jh/g) and Energy of a Single Ball (J) for Different Milling Conditions.

was not heat-treated. It can also be observed that the saturation magnetization is increased in the case of the annealed sample, which proves that heat treatment and the release of stress introduced to the powder during the milling process can positively affect the magnetic properties of the milled magnetic alloys.

For the next step, we sintered the annealed and un-annealed amorphous powders using two different temperatures of 470 °C and 510 °C to study the effect of annealing on the magnetic properties of samples sintered from heat-treated powder. To our surprise, the coercivity values of samples sintered from heat-treated powder were higher than samples sintered from non-heat-treated powder (for samples sintered at both 470 and 510 °C) even though the coercivity values were quite close to each other (Fig. 10). The difference in the coercivity values can be explained by the higher intensity of Fe$_2$B and Fe$_{23}$B$_6$ peaks from the XRD patterns and the slightly higher volume fraction of these two phases of the samples sintered from the annealed powder. Additionally, we studied the crystallite size and microhardness of samples sintered from heat-treated and non-heat-treated powders. Table 1 shows that the crystallite size of samples sintered from heat-treated powder is slightly higher than the sample sintered from regular powder. This difference in the crystallite size can explain the lower microhardness values observed in samples sintered from annealed powder since, according to the Hall-Petch relationship, microhardness and crystallite size are inversely correlated. According to Kotan et al. [37], the slope of their Hall-Petch plot is negligible when the crystallite sizes are in the range of nanometers. This can explain why only a slight change was observed in the microhardness values of our samples.

3.5. Spark plasma sintering at high pressure and low temperature

Spark plasma sintering processing parameters (pressure, holding time, and temperature) play an important role in affecting the microstructure, mechanical, and magnetic properties of metallic alloys. Four types of FeSiB powder alloys (two amorphous and two non-amorphous) were used for SPS experiments. The fully amorphous powder (milled for 30 h with BPR 10:1, 3 mm balls, and rotation speed of 700 rpm) was divided into two groups; one was heat treated, and the other one was not (our two amorphous powders), and each group was sintered at two sintering temperatures of 470 °C and 510 °C. The two non-amorphous powders chosen for these experiments were milled for 10h with BPR 5:1, 5 mm balls at a 700-rpm rotation speed and milled for 10h with BPR 5:1, 3 mm balls and 700 rpm rotation speed and then sintered at 470 °C.

Fig. 7 shows the XRD patterns of all sintered samples, and from this, it can be observed that more intense peaks of Fe$_2$B and Fe$_{23}$B$_6$ phases are present in samples that were sintered at a temperature of 510 °C in comparison with samples sintered at 470 °C. These peaks are broader in the case of samples sintered at 470 °C from an amorphous powder and almost non-existent in case of samples sintered at 470 °C from a non-amorphous powder. Formation of the secondary boron phases can be attributed to higher sintering temperatures surpassing the crystallization temperature of these two phases. Formation of Fe$_2$B and Fe$_{23}$B$_6$ phases at sintering temperatures higher than 500 °C is expected since α-Fe$_2$B forms between 496 °C and 642 °C [38], and Fe$_{23}$B$_6$ can form at temperatures even lower than that [39]. Table 1 shows the crystallite size and microhardness values of six sintered samples. For powders that

Table 1
Microhardness and crystallite size values for FeSiB sintered samples.

Condition	Crystallite Size (nm)	Microhardness (HV)
10h-3mm-470-5to1	19.41 ± 0.12	694.2 ± 10
10h-5mm-470-5to1	18.44 ± 0.02	974.5 ± 12
30h-3mm-470-10to1	10.37 ± 0.01	1176 ± 20
30h-3mm-470-10to1 (HT)	12.67 ± 0.37	1167 ± 15
30h-3mm-510-10to1	13.83 ± 0.23	1127 ± 13
30h-3mm-510-10to1 (HT)	14.98 ± 0.25	1122 ± 10

Table 2
Mechanical alloying conditions.

| Ball Size (mm)	BPR	Rotation Speed (RPM)	Milling Duration (h)	Eb	Et
5	10:01	700	10	0.0227	2462.13
5	5:01	700	10	0.02289	1249.81
3	5:01	700	10	0.0043	1137.02
3	5:01	700	20	0.0043	2274.05
5	10:01	700	20	0.0227	4924.26
5	5:01	700	20	0.02289	2499.62
3	10:01	700	10	0.00401	2094.94
3	10:01	700	20	0.00401	4189.89
5	15:01	700	10	0.0226	3678.93
3	10:1	700	30	0.004	6284.83
5	10:1	700	30	0.0227	7386.39
3	15:01	700	10	0.00362	2837.03
3	15:01	700	20	0.00362	5674.07
3	10:1	350	30	0.001	785.604
3	10:1	350	60	0.001	1571.209
3	10:1	350	90	0.001	2356.81
3	10:1	350	120	0.001	3142.418
3	15:1	350	60	0.0009	2127.77
3	15:1	350	90	0.0009	3191.66
3	15:1	350	120	0.0009	4255.55
3	10:1	500	60	0.002	4580.78
3	10:1	500	90	0.002	6871.17
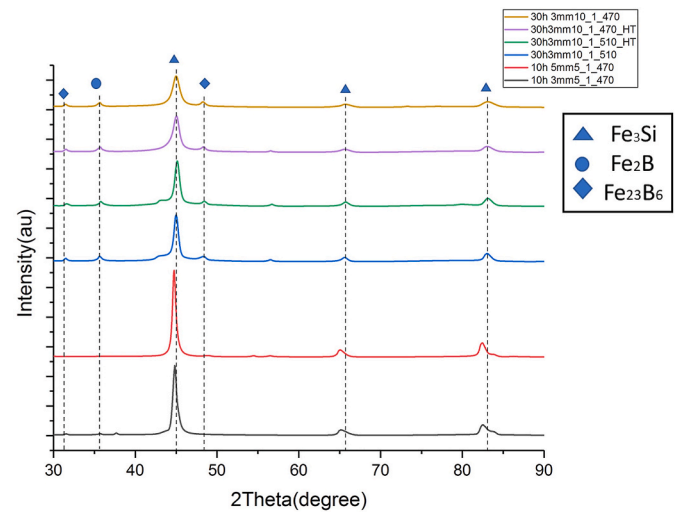
Fig. 7. XRD pattern of spark plasma sintered samples milled and sintered under different conditions.

were mechanically alloyed under the same condition, the higher sintering temperature resulted in bigger crystallite size and lower microhardness values, which is explainable by the Hall-Petch relation.

3.6. Scanning electron microscopy (SEM) analysis of SPS samples

SEM images of spark plasma sintered samples are depicted in Fig. 8. The samples were mechanically alloyed and spark plasma sintered under the following conditions: 30h-milled_3 mm balls_10:1 BPR sintered at 510 °C, 30h-milled_3 mm balls_10:1 BPR heat treated, then sintered at 510 °C, 30h-milled_3 mm balls_10:1 BPR sintered at 470 °C, 30h-milled_3 mm balls_10:1 BPR, heat treated then sintered at 470 °C, 10h-milled_3 mm balls_5:1 BPR sintered at 470 °C and 10h-milled_5 mm balls_5:1 BPR sintered at 470 °C. It can be observed from Fig. 8 that the 10h-milled samples show much coarser microstructure in comparison to samples that were milled for 30 h. This can be attributed to smaller powder particles from which the 30-h samples were sintered. The non-homogeneous and coarse microstructure of samples that were milled for the shorter duration of 10 h can also be attributed to lower levels of
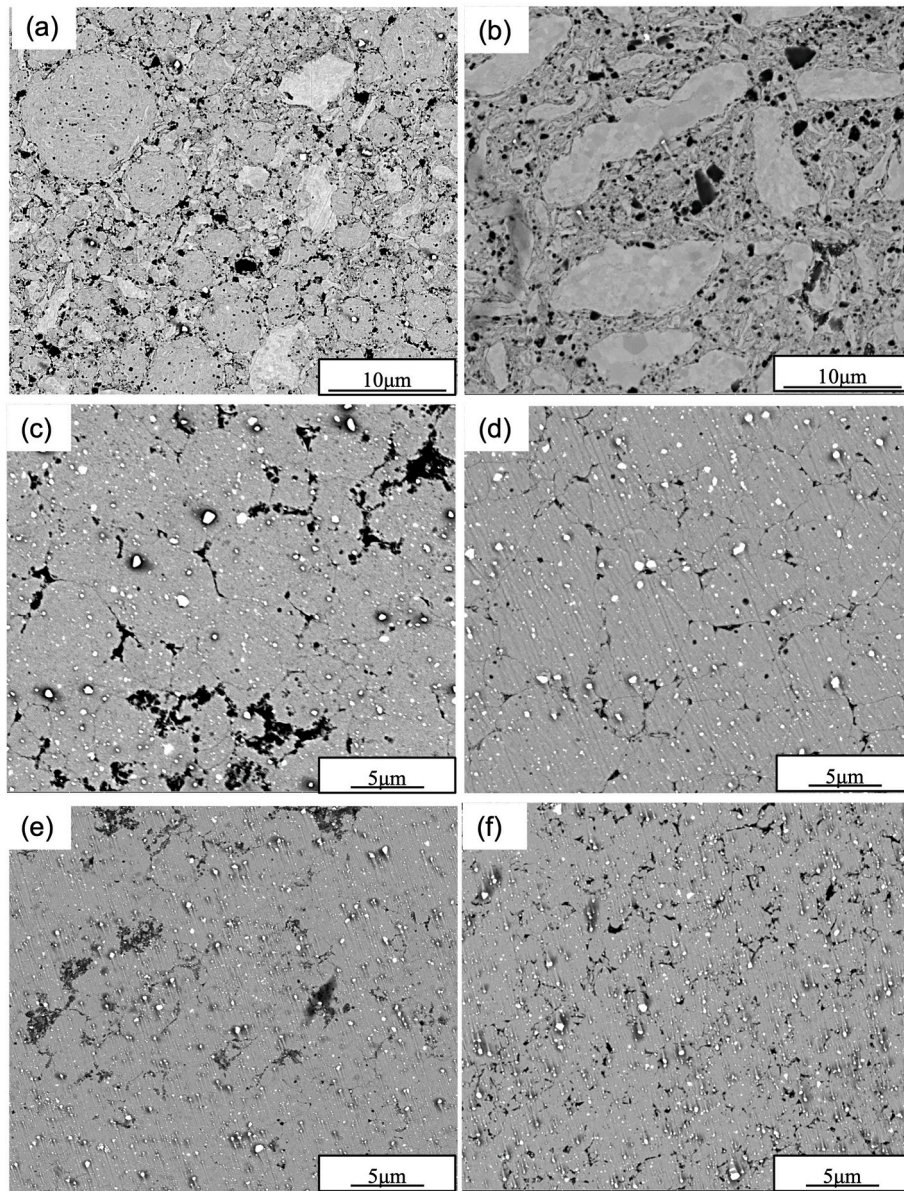
Fig. 8. SEM images of sintered FeSiB samples. (a) and (b): 10h-milled_3 mm balls_5:1 BPR sintered at 470 °C and 10h-milled_5 mm balls_5:1 BPR sintered at 470 °C. (c) and (d): 30h-milled_3 mm balls_10:1 BPR sintered at 470 °C and 30h-milled_3 mm balls_10:1 BPR, heat treated then sintered at 470 °C, (e) and (f): 30h-milled_3 mm balls_10:1 BPR sintered at 510 °C and 30h-milled_3 mm balls_10:1 BPR heat treated then sintered at 510 °C.

alloying due to limited milling time in these samples compared to samples that were milled for 30 h. From Fig. 8, it can also be observed that when two samples that were sintered under the same sintering parameters and from the same powder (one sintered from heat-treated powder and one from not heat-treated powder) are compared, the heat-treated sample shows only a slight difference in the microstructure in terms of homogeneity and grain size. Another observation from Fig. 8 is the coarser microstructure of heat-treated and non-heat-treated samples that were sintered at 510 °C. Given the fact that the initial powders (heat treated or not) of all the 30-h milled samples were the same, the observed difference is due to higher sintering temperature, which ultimately increases the grain sizes and coarsens the microstructure. These observations can confirm that the microstructure of SPS-processed samples is influenced by the type of powder from which it is sintered. Therefore, milling duration can directly impact the microstructure of consolidated powder; however, heat treating the initial powder does not affect the microstructure of the resultant sample much.

3.7. Magnetic properties of powder and sintered samples

Different factors, such as the chemical composition of the alloy and the magnetostriction and magnetic anisotropy of a magnetic alloy, can affect its magnetic properties [40]. Figs. 9 and 10 show the magnetization versus the applied magnetic field measured at room temperature. The saturation magnetization (M_s) values resulting from our experiments are high compared to the findings of other researchers, and the coercivity values are reasonable. The highest saturation magnetization obtained from our experiments was 182.8 emu/g for powder and 172.7 emu/g for sintered samples. The coercivity values observed in the samples milled with the higher rotation speed of 700 rpm and shorter milling duration of only up to 30 h were proven to be lower than those of samples that were milled for longer durations at lower rotation speeds. The lowest coercivity value previously obtained from our experiments was 62.4 Oe, whereas the coercivity values of samples milled with high rotation speed are as low as 33.4 Oe [8].

Other researchers who have studied similar compositions have
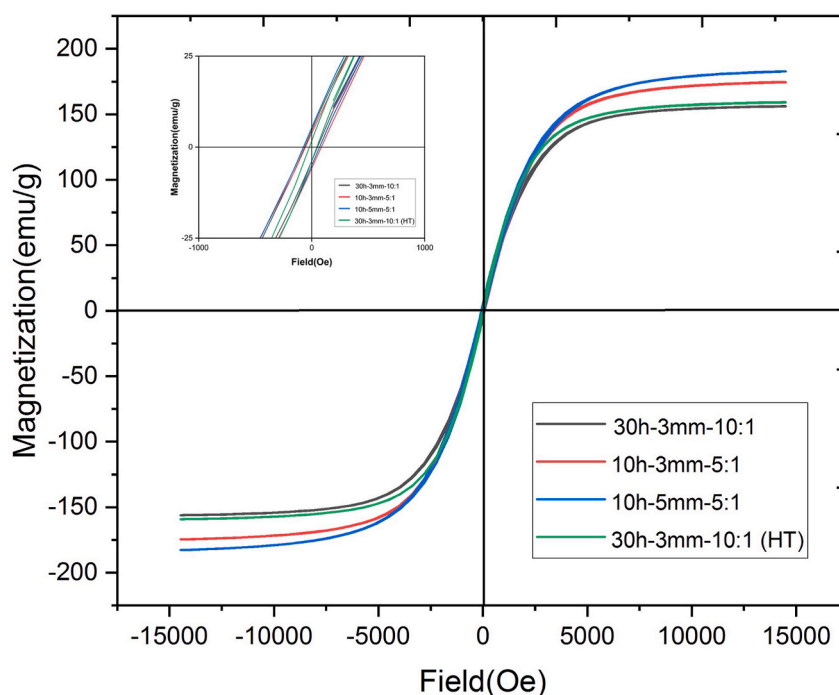
Powder Sample	Ms (emu/g)	Hc (Oe)
7. 30h_3mm_10:1	156.1	56.9
8. 10h_3mm_5:1	174.6	74.2
9. 10h_5mm_5:1	182.8	78.7
10. Heat treated (30h-3mm-10:1)	159.2	44.9

Fig. 9. Magnetization and coercivity values of mechanically alloyed FeSiB samples under different milling conditions and heat treatment.

obtained saturation magnetizations lower than what we got from our present investigation [29,41,42]. The reason for the higher saturation magnetization observed from our experiments is due to alloying with optimized parameters as well as refinement of powder with nano-crystalline grain structure [43]. SPS-processed samples sintered from amorphous powder milled with BPR 0:1, rotation speed of 700 rpm for 30 h had M_s values in the range of 152.6–158.1 emu/g. Similarly, the amorphous powder samples (milled with 700 rpm, BPR 10:1 for 30 h), one annealed and one not annealed, show magnetic properties that are close together. However, there are more drastic differences in samples' magnetic properties when milled with different parameters. For instance, the saturation magnetization range of 152–158 emu/g can be increased to 174–182 emu/g by altering the BPR and milling duration. Even if we compare two powders that were both milled with the same milling duration and ball-to-powder ratio (e.g., 10h milling duration and BPR 5:1) with the only difference being the size of the milling balls, a significant difference in the magnetic properties of the samples has been observed than if two powders were milled under the same condition with the only difference being the heat treatment. Therefore, it can be concluded that the mechanical alloying processing parameters are more influential on the magnetic properties of FeSiB-based alloys than annealing heat treatment.

The coercivity values of mechanically alloyed samples are depicted in Fig. 9. The coercivity values for samples milled for 10 h, the ball-to-powder ratio of 5:1, and ball sizes of 3 and 5 mm are very close together, with the 5 mm milled sample having a slightly higher

coercivity. This higher coercivity value is due to the higher intensity of Fe_2B and $Fe_{23}B_6$ boron peaks (based on XRD results) observed in powder alloy milled with 5 mm balls compared to powder alloy milled with 3 mm balls. These boron phases act as pinning sites for magnetic domains and, therefore, deteriorate the magnetization value. The saturation magnetization of the 10h, 5:1 sample is higher than the 30h and 10:1 sample, which might be due to the presence of a large volume fraction of Fe_3Si phase in the samples sintered from these powder alloys. The same can be said for the comparison between the 10h, 5:1, 5 mm and the 10h, 5:1, 3 mm samples, where the saturation magnetization value is higher in the case of the 5 mm sample. From the XRD patterns, it can be seen that these 2 samples have a higher volume fraction of the Fe_3Si phase. The higher saturation magnetization in the case of 10h_3 mm_5:1 and 10h_5 mm_5:1 samples sintered at 470 °C can be attributed to dispersion of large volume fraction of Fe3Si particles in the amorphous matrix, which results in increased saturation magnetization [44].

4. Conclusions

FeSiB-based alloys were processed using mechanical alloying followed by spark plasma sintering. The effect of different mechanical alloying processing parameters and sintering temperature on the microstructure and mechanical and magnetic properties of FeSiB alloy was investigated. Additionally, the total amount of energy introduced to the powder during the mechanical alloying process, as well as the energy of a single milling ball, was calculated and based on these calculations
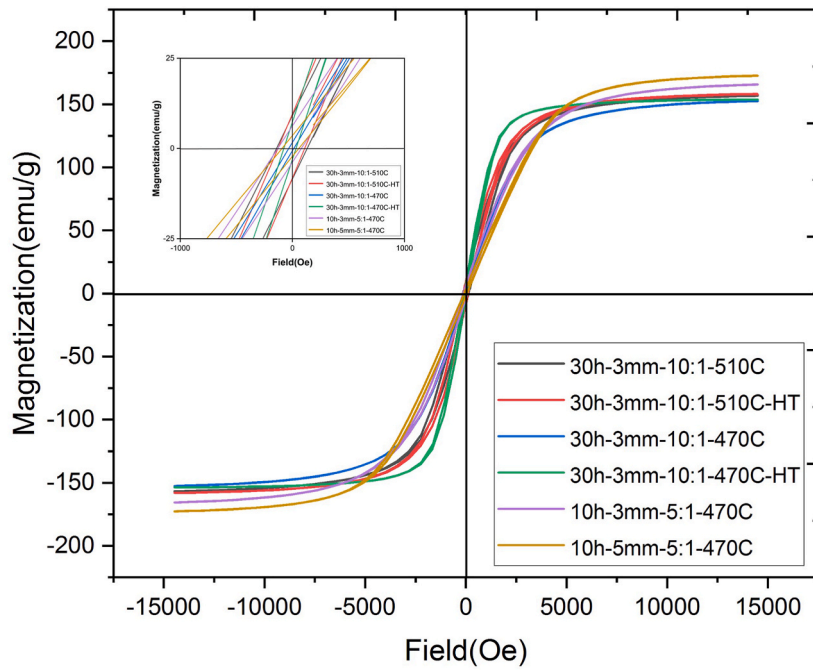
SPS Sample	Ms (emu/g)	Hc (Oe)
1. 30h_3mm_10:1_510 °C	156.9	137.0
2. 30h_3mm_10:1_510 °C_HT	158.1	139.1
3. 30h_3mm_10:1_470 °C	152.6	33.4
4. 30h_3mm_10:1_470 °C_HT	153.7	46.5
5. 10h_3mm_5:1_470 °C	165.6	99.7
6. 10h_5mm_5:1_470 °C	172.7	65.6

Fig. 10. Magnetization and coercivity values for mechanically alloyed FeSiB samples under different heat treatment, milling, and SPS conditions.

and the results from x-ray diffraction, a window of energy in which FeSiB-based alloys show amorphous structure was determined. The conclusions from our experiments are as follows.

- Samples sintered from annealed powder exhibited higher saturation magnetization than samples sintered from non-annealed powder but also showed higher coercivity values.
- Annealed powder showed lower coercivity compared to the un-annealed powder sample. This behavior is the opposite of sintered samples.
- Higher saturation magnetization and lower coercivity were obtained for alloys milled with larger milling balls.
- To reach amorphization, a minimum energy for a single ball is required, even if the total energy of the process is within the amorphization window.
- Mechanical alloying processing parameters have a more significant effect on the magnetic properties of FeSiB-based alloys than heat treatment.
- The window for the total energy introduced to the powder during the mechanical alloying process of FeSiB-based alloys in which amorphization takes place is 2462–7386 Jh/g, and the minimum impact energy of a single ball required for amorphization is 0.0029J.

CRediT authorship contribution statement

T. Larimian: Writing – original draft, Investigation, Formal analysis, Conceptualization. **V. Chaudhary:** Writing – review & editing, Investigation, Formal analysis. **R.K. Gupta:** Investigation, Formal analysis. **R. V. Ramanujan:** Investigation, Formal analysis. **T. Borkar:** Writing – review & editing, Resources, Project administration, Investigation, Funding acquisition, Conceptualization.

Declaration of competing interest

The authors declare that they have no known competing financial interests or personal relationships that could have appeared to influence the work reported in this paper.

Acknowledgments

Data availability

Data will be made available on request.

References

[1] R. Hasegawa, Present status of amorphous soft magnetic alloys, J. Magn. Magn Mater. 215 (2000) 240–245.

[2] R. Jha, D.R. Diercks, A.P. Stebner, C.V. Ciobanu, Metastable phase diagram and precipitation kinetics of magnetic nanocrystals in FINEMET alloys, arXiv (2017) 1709–8306.

[3] Z. Li, K. Yao, D. Li, X. Ni, Z. Lu, Core loss analysis of Finemet type nanocrystalline alloy ribbon with different thickness, Prog. Nat. Sci.: Mater. Int. 27 (5) (2017) 588–592.

[4] M.E. McHenry, M.A. Willard, D.E. Laughlin, Amorphous and nanocrystalline materials for applications as soft magnets, Prog. Mater. Sci. 44 (4) (1999) 291–433.

[5] V.A. Kataev, Y.N. Starodubtsev, K.O. Bessonova, Magnetizing of Finemet-type alloys by magnetization rotation in weak fields, J. Phys.: Conf. Ser. 1389 (1) (2019) 012120.

[6] T. Gheiratmand, H.M. Hosseini, Finemet nanocrystalline soft magnetic alloy: investigation of glass forming ability, crystallization mechanism, production techniques, magnetic softness and the effect of replacing the main constituents by other elements, J. Magn. Magn Mater. 408 (2016) 177–192.

[7] Y.A. Yoshizawa, S. Oguma, K. Yamauchi, New Fe-based soft magnetic alloys composed of ultrafine grain structure, J. Appl. Phys. 64 (10) (1988) 6044–6046.

[8] T. Larimian, V. Chaudhary, J. Christudasjustus, R.V. Ramanujan, R. Gupta, T. Borkar, Bulk-nano spark plasma sintered Fe-Si-B-Cu-Nb based magnetic alloys, Intermetallics 124 (2020) 106869.

[9] T. Larimian, V. Chaudhary, M.U.F. Khan, R.V. Ramanujan, R.K. Gupta, T. Borkar, Spark plasma sintering of Fe–Si–B–Cu–Nb/Finemet based alloys, Intermetallics 129 (2021) 107035.

[10] T. Liu, M. Wang, Z. Zhao, High-frequency properties of $Fe_{73.5}Cu_1Nb_3Si_{13.5}B_9/$ $Zn_{0.5}Ni_{0.5}Fe_2O_4$ soft magnetic composite with micro-cellular structure, Sci. China Phys. Mech. Astron. 55 (2012) 2392–2396.

[11] S. Lee, H. Kato, T. Kubota, A. Makino, A. Inoue, Fabrication and soft-magnetic properties of Fe–B–Nb–Y glassy powder compacts by spark plasma sintering technique, Intermetallics 17 (4) (2009) 218–221.

[12] S. Sharma, R. Vaidyanathan, C. Suryanarayana, Criterion for predicting the glass-forming ability of alloys, Appl. Phys. Lett. 90 (11) (2007).

[13] B. Movahedi, M.H. Enayati, C.C. Wong, Study on nano crystallization and amorphization in Fe–Cr–Mo–B–P–Si–C system during mechanical alloying, Mater. Sci. Eng. B 172 (1) (2010) 50–54.

[14] Q.J. Chen, H.B. Fan, L. Ye, S. Ringer, J.F. Sun, J. Shen, D.G. McCartney, Enhanced glass forming ability of Fe–Co–Zr–Mo–W–B alloys with Ni addition, Mater. Sci. Eng. A 402 (1–2) (2005) 188–192.

[15] H.S. Chen, Glassy metals, Rep. Prog. Phys. 43 (4) (1980) 353.

[16] E. Fechová, P. Kollar, J. Füzer, J. Kováč, P. Petrovič, V. Kavečanský, The influence of the long time milling on the structure and magnetic properties of the Fe–Cu–Nb–Si–B powder, Mater. Sci. Eng. B 107 (2) (2004) 155–160.

[17] C. Suryanarayana, Mechanical alloying and milling, Prog. Mater. Sci. 46 (1–2) (2001) 1–184.

[18] T. Voisin, L. Durand, N. Karnatak, S. Le Gallet, M. Thomas, Y. Le Berre, J. Castagne, A. Couret, Temperature control during Spark Plasma Sintering and application to up-scaling and complex shaping, J. Mater. Process. Technol. 213 (2) (2013) 269–278.

[19] T. Gheiratmand, H.M. Hosseini, P. Davami, C. Sarafidis, Fabrication of FINEMET bulk alloy from amorphous powders by spark plasma sintering, Powder Technol. 289 (2016) 163–168.

[20] Z. Xiao, C. Tang, H. Zhao, D. Zhang, Y. Li, Effects of sintering temperature on microstructure and property evolution of $Fe_{81}Cu_2Nb_3Si_{14}$ soft magnetic materials fabricated from amorphous melt-spun ribbons by spark plasma sintering technique, J. Non-Cryst. Solids 358 (1) (2012) 114–118.

[21] B.V. Neamțu, T.F. Marinca, I. Chicinaș, O. Isnard, F. Popa, P. Păşcuţă, Preparation and soft magnetic properties of spark plasma sintered compacts based on Fe–Si–B glassy powder, J. Alloys Compd. 600 (2014) 1–7.

[22] A.W. Weeber, H. Bakker, Amorphization by ball milling. A review, Phys. B Condens. Matter 153 (1–3) (1988) 93–135.

[23] C.C. Koch, O.B. Cavin, C.G. McKamey, J.O. Scarbrough, Preparation of "amorphous''Ni60Nb40 by mechanical alloying, Appl. Phys. Lett. 43 (11) (1983) 1017–1019.

[24] E. Hellstern, L. Schultz, Amorphization of transition metal Zr alloys by mechanical alloying, Appl. Phys. Lett. 48 (2) (1986) 124–126.

[25] R.B. Schwarz, R.R. Petrich, C.K. Saw, The synthesis of amorphous Ni Ti alloy powders by mechanical alloying, J. Non-Cryst. Solids 76 (2–3) (1985) 281–302.

[26] G. Veltl, B. Scholz, H.D. Kunze, Amorphization of Cu Ta alloys by mechanical alloying, Mater. Sci. Eng. A 134 (1991) 1410–1413.

[27] B.S. Murty, S.J.M.R. Ranganathan, Novel materials synthesis by mechanical alloying/milling, Int. Mater. Rev. 43 (3) (1998) 101–141.

[28] C. Suryanarayana, G.H. Chen, A. Frefer, F.H. Froes, Structural evolution of mechanically alloyed Ti Al alloys, Mater. Sci. Eng. A 158 (1) (1992) 93–101.

[29] B.V. Neamțu, H.F. Chicinaș, T.F. Marinca, O. Isnard, O. Panä, I. Chicinaș, Amorphisation of Fe-based alloy via wet mechanical alloying assisted by PCA decomposition, Mater. Chem. Phys. 183 (2016) 83–92.

[30] A. Nouri, C. Wen, Surfactants in mechanical alloying/milling: a catch-22 situation, Crit. Rev. Solid State Mater. Sci. 39 (2) (2014) 81–108.

[31] S. Torkan, A. Ataie, H. Abdizadeh, S. Sheibani, Effect of milling energy on preparation of nano-structured Fe70Si30 alloys, Powder Technol. 267 (2014) 145–152.

[32] J. Joardar, S.K. Pabi, B.S. Murty, Milling criteria for the synthesis of nanocrystalline NiAl by mechanical alloying, J. Alloys Compd. 429 (1–2) (2007) 204–210.

[33] M. Magini, A. Iasonna, Energy transfer in mechanical alloying (overview), Mater. Trans. JIM 36 (2) (1995) 123–133.

[34] N. Burgio, A. Iasonna, M. Magini, S. Martelli, F. Padella, Mechanical alloying of the Fe– Zr system. Correlation between input energy and end products, II. nuovo. cimento. D. 13 (4) (1991) 459–476.

[35] J. Peng, J. Yang, T. Zhang, X. Song, Y. Chen, Preparation and characterization of Fe substituted $CoSb_3$ skutterudite by mechanical alloying and annealing, J. Alloys Compd. 381 (1–2) (2004) 313–316.

[36] A.K. Sinha, M.N. Singh, A. Upadhyay, M. Satalkar, M. Shah, N. Ghodke, S.N. Kane, L.K. Varga, A correlation between the magnetic and structural properties of isochronally annealed Cu-free FINEMET alloy with composition $Fe_{72}B_{19.2}Si_{4.8}Nb_4$, Appl. Phys. A 118 (2015) 291–299.

[37] H. Kotan, M. Saber, C.C. Koch, R.O. Scattergood, Effect of annealing on microstructure, grain growth, and hardness of nanocrystalline Fe–Ni alloys prepared by mechanical alloying, Mater. Sci. Eng. A 552 (2012) 310–315.

[38] E.C. Passamani, J.R.B. Tagarro, C. Larica, A.A.R. Fernandes, Thermal studies and magnetic properties of mechanical alloyed Fe2B, J. Condens. Matter Phys. 14 (8) (2002) 1975.

[39] J. Long, P.R. Ohodnicki, D.E. Laughlin, M.E. McHenry, T. Ohkubo, K. Hono, Structural studies of secondary crystallization products of the $Fe_{23}B_6$-type in a nanocrystalline FeCoB-based alloy, J. Appl. Phys. 101 (9) (2007).

[40] M.M. Raja, K. Chattopadhyay, B. Majumdar, A. Narayanasamy, Structure and soft magnetic properties of Finemet alloys, J. Alloys Compd. 297 (1–2) (2000) 199–205.

[41] T. Gheiratmand, H.M. Hosseini, P. Davami, C. Sarafidis, Fabrication of FINEMET bulk alloy from amorphous powders by spark plasma sintering, Powder Technol. 289 (2016) 163–168.

[42] S. Alleg, S. Kartout, M. Ibrir, S. Azzaza, N.E. Fenineche, J.J. Suñol, Magnetic, structural and thermal properties of the Finemet-type powders prepared by mechanical alloying, J. Phys. Chem. Solids 74 (4) (2013) 550–557.

[43] R.C. O'handley, Modern Magnetic Materials: Principles and Applications, Wiley-VCH, 1999, p. 768.

[44] A.R. Yavari, O. Drbohlav, Thermodynamics and kinetics of nanostructure formation in soft-magnetic nanocrystalline alloys (overview), Mater. Trans. JIM 36 (7) (1995) 896–902.